LHCb 2001-025 Muon
28 March 2001

Beam tests of WPC-8 and WPC-9 prototypes of the wire pad chambers for the LHCb Muon System

B.Bochin, S.Guets, V.Lazarev, N.Saugidova, E.Spiridenkov, An.Vorobiev, A.Vorobyov

Petersburg Nuclear Physics Institute

Abstract

Two new prototypes, WPC-8 and WPC-9, of the Wire Pad Chambers have been constructed at PNPI. The design of these double-gap wire chambers was similar to the previously tested WPC-7 prototype with one important difference: the anode wire planes were electrically independent, which allows to operate the new prototypes either in the double-gap or in the single-gap modes. The prototypes have been tested in the T11 beam at CERN, and this report presents the results of the tests. As in the previous tests, the PNPI front-end electronics based on the discrete elements was used in the read out channels. In addition, a new option of the FE electronics based on the SONY chip has been developed (SONY++) with an active adapter at the input of the chip allowing to reduce the input impedance and the width of the shaped signals. The SONY++ option was tested with the WPC-9 prototype with very satisfactory results. The performance proved to be identical to that with the PNPI FE electronics.

1. Introduction

In our previous note [1], a detailed report was presented on the beam tests of the WPC-7 prototype of the wire pad chambers for the LHCb Muon System. It was a two-gap chamber with the electrically connected wire planes from both gaps. The WPC-7 prototype demonstrated a very good performance with the efficiency plateau (≥95% efficiency in a 20 ns time window) varying from 500 V for 4x16 cm^2 wire pads to 400 V for 12x16 cm^2 wire pads operating with the nominal gas mixture of Ar(40%) + CO_2(50%) + CF_4(10%).

The described here new prototypes WPC-8 and WPC-9 had the same gap width, wire spacing, and wire diameters as the WPC-7 prototype. The main difference was the electrically separated wire planes allowing operating two gaps independently. As in our previous tests, the PNPI front-end electronics based on discrete elements was used in the read out channels. In addition, a modified SONY chip FE version was tested with an active adapter at the input of the chip designed to decrease the input impedance of the SONY chip and to reduce the width of the output signal. The WPC-8 and WPC-9 prototypes have been tested in the T11 pion beam at CERN during the test run in October 2000.

Here we report on the results of these tests.

2. Design of WPC-8 and WPC-9 prototypes

Figure 1 shows a schematic view of the prototypes. These are double-gap chambers with the sensitive area of 16x24 cm^2. The wires are wound along the short side and grouped together to form two pads of 4x16 cm^2 size and two pads of 8x16 cm^2 size in each wire plane. The geometry parameters are as in the previous prototypes:

Distance between the cathodes −5.00 mm in each gap.
Anode wire spacing −1.50 mm.
Anode wire diameter −30 μm.
Anode wire tension −30 g.

The WPC-8 and WPC-9 prototypes had slightly different shapes of the anode wire fixation bars as shown in Fig1. Also, there was some difference in the geometry of the guard wires: WPC-9 contained two guard wires of 90 μm in diameter in both gaps, while WPC-8 contained two guard wires in one gap and one guard wire in the other gap (Figure1).

One side of each wire pad was connected to a common HV bus through a 1.5 MΩ resistor. The other side of each wire pad was connected

through a 1000 pF decoupling capacitor to a preamplifier (single-gap option, Fig2b). Also, it was possible to connect two opposite wire pads to one preamplifier as shown in Figure 2a (double-gap option).

3. Electronics

There were two options of the front-end electronics. First, both prototypes were equipped with the PNPI FE based on discrete elements and consisting of a preamplifier followed by the main amplifier as described in [1]. In this option, the input impedance was 30 Ω plus 20 Ω from the diode protection circuit, the rise time of the shaped real signals was about 15 ns in the "Fast" channel connected to a discriminator for time measurements and about 20 ns in the "Slow" channel connected to an ADC for charge measurements (see [1]).

In addition, we investigated a possibility to use the FE electronics based on the SONY chip. Unfortunately, direct application of the SONY chip as the preamplifiers in the LHCb muon chambers revealed several problems: large input impedance (80 Ω), relatively long signal (~200 ns full width), not sufficient amplification factor resulted in a worse time resolution, larger cross-talks, and a larger dead time in comparison with the PNPI front-end electronics considered at present as a reference satisfying quite well the requirements of the LHCb experiment. Therefore, we developed a modification (SONY++) where an active adapter was added in front of the SONY chip designed in such a way that the input impedance was reduced to 25 Ω, the amplification factor was increased by a factor of 3, the signal full length was reduced to 60 ns, and the tail cancellation was provided. The active adapter was quite simple, it consisted of 2 transistors, 7 resistors, and 5 capacitors in each channel. Each SONY chip contained 4 channels with digital and analog outputs. The digital signals were sent through the LVDS $\rightarrow$ ECL converters to TDCs for time measurements while the analog signals were used for charge measurements. The SONY++ option was installed on the WPC-9 prototype operating in the double-gap mode (Figure 3), and the beam tests were carried out at the end of the running period.

4. Experimental setup

The tests were carried out at CERN in a 3 GeV/c negative pion beam at PS. The layout of the experiment is shown in Figure 4. Beam particles were detected with two scintillator counters: S1 (15 cm x 15 cm) and S2 (20 cm x 20 cm). The coincidence between these two counters in a 10 ns window provided a trigger signal:

TR1 = S1 x S2.

The constant-fraction discriminators (CFD) were used in both S1 and S2 channels helping to reduce the time jitter of the trigger signal down to ≤1 ns. The beam particles were detected also by two planes (H-horizontal and V-vertical) of the hodoscope counters, each plane containing 8 counters (1 cm x 8 cm). The following information was registered by the acquisition system:

- Time arrivals and amplitudes of the signals from the S1 and S2 scincillator counters measured with TDCs and ADCs.
- Time arrivals of the signals from all hodoscope counters measured with TDCs.
- Time arrivals of the signals from the WPC measured with TDCs.
- Integrated current signals from the WPC measured with ADCs.

In addition, there was ungated data from the scalers detecting signals from all scintillator counters and from the WPC FAST channels. The scalers provided two types of information: the total number of counts during the beam spill and the number of counts during a 330 ms interval in-between the beam spills. The beam spill was around 330 ms.

The WPC was installed on a movable platform allowing to vary the beam position over the chamber area. The gas mixture was $Ar(40\%)+CO_2(50\%)+CF_4(10\%)$. It was provided with a new automated gas mixing system which was properly calibrated before the experiment. In all these measurements, the beam intensity was around $5 \cdot 10^4$ particles per spill. The beam size was about 5 cm in diameter.

5. Data analysis and results

The PNPI FE electronics was described in detail in ref [1]. Figure 3b displays the shape of the signals at the analog outputs of the SONY++ chip. These signals proved to be nearly identical to those at the FAST output of the PNPI FE electronics as can be seen from Table1.

Table 1. Comparison of the signal parameters at the output of the SONY++ and PNPI FE electronics.

Pad size cm^2	SONY++		PNPI	
	rise time, ns	full width, ns	rise time, ns	full width, ns
4x16	13	53	14	65
8x16	19	70	16	70

Depending on the pad size, the rise time (from 10% to 90% of the amplitude) was found to be 13 ns to 19 ns, and the full width (from 10% to 10% of the amplitude) varied from 50 ns to 70 ns. Figure3b demonstrates also the quality of the tail cancellation.

The ADC and TDC spectra were measured using the same event selection algorithm as in [1]:

- Cut1. Shower rejection.
  Large amplitudes in the ADC spectra from the S1 and S2 counters were rejected. The pile-ups of two and more particles in the 20ns time window were rejected in this way. Typically, about 10% of the events were rejected by this cut. The remaining events were considered as TR2-events.
- Cut2. Hodoscope selection.
  - Only signals in a 20 ns time window in the TDC spectra were selected. There should be one and only one signal both in the H-plane and in the V-plane of the Hodoscope. This helps to kill further the showers in the beam. A certain combination of the hodoscope counters could be selected to define a beam spot.

The events passing Cut1 and Cut2 were considered as TR3-events. No cuts have been applied to the signals from WPC.

The number of the TR3-events was used in calculations of the efficiencies in the analog and digital channels of WPC:

$$\mathrm{Eff}_{\mathrm{ADC}} = \sum_{i=350}^{overflow} N_i(\mathrm{ADC}) \Big/ \sum \mathrm{TR3} \qquad (1)$$

$$\mathrm{Eff}_{\mathrm{TDC}} = \sum_{t1}^{t1+\Delta t} N_i(\mathrm{TDC}) \Big/ \sum \mathrm{TR3} \qquad (2)$$

The hodoscope selection guaranteed that at least 99% of the selected particles were inside the pad size. This value was controlled by the ADC efficiency determined according to expression (1).While filling the TDC

histogram, at least one hit in the time window from 240 ns to 290 ns was required. When more than one hit were observed in this window, only one of them (first arrival) was included in the histogram. However, the frequency of such double-hit events was quite low (<1%). From the time distributions, the following quantities were obtained: <t>, r.m.s.(t), and the registration efficiencies in various time windows (50 ns, 25 ns, 20 ns, 15 ns) calculated using expression (2).

5.1 Noise counting rates

Figure 5 presents the noise counting rates measured between the beam spills in a 330 ms time window for various HV-values. The measurements were performed with the WPC-8 and WPC-9 prototypes operating in the separate gaps mode with the PNPI FE electronics and the discriminator thresholds set to 45 mV. Such measurements determine the highest HV-values with stable operation of the wire chamber. One can see from Figure 5 that HV_{max}=3.35 kV for both prototypes with slightly worse performance of the gap B in WPC-8. This might be related to the wire guard geometry: only one guard wire was used in this gap while two guard wires were used in gap A of WPC-8 and in both gaps of WPC-9.

The measured HV_{max}=3.35 kV should be compared with HV_{max}=3.45 kV obtained in the previous tests of WPC-7 [1]. To understand the reason for this difference, we repeated the measurements with WPC-7 and obtained HV_{max}=3.40 kV. The 50V difference with the previous measurements could be explained by the difference in the atmospheric pressure (1030 mb during the previous test run, 1000 mb in the present measurements) and also by some possible difference in the gas mixture, as a new gas mixture system was used in the present tests. Note that the efficiency plateau in WPC-7 remained practically unchanged (compare Table2 with Table 2 from [1]). Still the remaining 50 V difference between HV_{max}=3.35 kV for the new prototypes and HV_{max}=3.40 kV for WPC-7 is not understood. Maybe it is due to some small differences in the chamber geometry parameters (gap width). What is important, the efficiency plateau in the new prototypes proved to be even slightly larger than in the WPC-7 prototype.

5.2 Time resolution and efficiency

Figures 6 and 7 display the amplitude and the time distributions of the signals from WPC-9 operating in the single-gap and the double-gap modes, respectively. The high voltage was adjusted so that the mean ADC became equal in both modes. The 150 V difference in HV corresponds to an increase in the gas gain by a factor of 2. As expected, the Landau distribution is less broad in the double-gap chamber with a cleaner space above the pedestal (pedestal=260 channel). On the other hand, the measured time distributions proved to be very similar (note, however, the difference in the HV-values).

More detail comparison of the time resolution achieved with WPC-9 operating either in the single-gap or in the double-gap modes is presented in Fig8. One can see from this figure that the double-gap mode improves the time resolution by a factor of $\sqrt{2}$ at the HV-values around 3 kV, while at the highest HV-values this factor becomes larger than $\sqrt{2}$.

Figures 9 and 10 compare the detection efficiency in a 20 ns time window for WPC-9 operating in the single-gap and double-gap modes. These figures show that, though the efficiency plateau is reduced by ~150 V in the single-gap mode, still it remains quite large. Therefore, it is very important to have independent high voltage suppliers for each gap: in case of troubles with one gap in the double-gap chamber, the other gap could provide nearly the required efficiency of ~95% thus increasing essentially the redundancy of the Muon System.

The measured efficiency plateau in the WPC-7, WPC-8, and WPC-9 prototypes operating in the single-gap and the double-gap modes are presented in Tables 2 to 6. As in [1], the HV_{min} is the high voltage where the detection efficiency in 20 ns time window exceeds 95%. The definition of HV_{max} is given in section 5.1 The efficiency plateau is determined as the difference HV_{max} - HV_{min}. The tables present also the atmospheric pressure during the measurements. Note that a 50 mb increase in the atmospheric pressure results in ~35% decrease in the gas gain. To compensate this gas gain decrease, one should increase the high voltage by ~50 V.

Comparison of the obtained results with our previous test results of the WPC-7 prototype [1] shows that in the all tested double-gap prototypes the efficiency plateau is practically the same. It is about 500 V for pad size of 4x16 cm^2 and 440 V for the pad size of 8x16 cm^2. When the chambers operate in the single-gap mode, the plateau is reduced by ~150 V.

Table 2. Efficiency plateau in the double-gap WPC-7 prototype. HV_{max} =3.4 kV.

Pad	Pad size	Thresh mV	HV_{min} kV	Plateau V	P mb
W2	8x16	30	3.0	400	1005

Table 3. Efficiency plateau in WPC-9 prototype operating in the double-gap mode. HV_{max} =3.35 kV.

Pad	Pad size	Thresh mV	HV_{min} KV	Plateau V	P mb
W3	4x16	30	2.88	470	1025
W3	4x16	45	2.94	410	1020
W2	8x16	30	2.92	430	1010
W2	8x16	45	2.97	380	1010

Table 4. Efficiency plateau in WPC-9 prototype operating in the single-gap mode. HV_{max} =3.35 kV.

Pad	Pad size	Thresh mV	HV_{min} KV	Plateau V	P mb
W3a,b	4x16	30	3.03	320	1030
W3a,b	4x16	45	3.12	230	1030
W2a,b	8x16	30	3.07	280	1025
W2a,b	8x16	45	3.12	230	1025

Table 5. Efficiency plateau in WPC-8 prototype operating in the double-gap mode. HV_{max} =3.35 kV.

Pad	Pad size	Thresh mV	HV_{min} KV	Plateau V	P mb
W3	4x16	30	2.85	500	995
W3	4x16	45	2.89	460	1000
W2	8x16	30	2.88	470	996
W2	8x16	45	2.92	430	1000

Table 6. Efficiency plateau in WPC-8 prototype operating in the single-gap mode. HV_{max} =3.35 kV.

Pad	Pad size	Thresh mV	HV_{min} kV	Plateau V	P mb
W2a,b	8x16	30	3.00	350	980
W2a,b	8x16	45	3.07	280	990

5.3 Cross-talk

The cross-talk probabilities for the double-gap WPC-7 have been described in detail in [1]. Here we present the cross-talks measured in WPC-9 operated in the single-gap mode. The definition of the cross-talk probability was as in [1]. The beam spot was selected to be inside one certain pad, and the signals were detected in the other TDC channels in the time interval $0 \leq t \leq 300$ns. Figure 11 demonstrates the cross-talk probabilities vs HV measured with the beam spot on the pad W2 (8x16 cm^2). Table 7 presents the cross-talk probabilities for some typical HV-values. We can comment on these results in the following way. Suppose one gap was switched out in the double-gap chamber, and the chamber continue to operate at the nominal for the double-gap mode HV^D_{nom}. In this case the cross-talk probability is reduced by a factor of 2. However, if we want to restore the chamber efficiency by increasing the high voltage to $HV^S_{nom} = HV^D_{nom} + 150V$, then the cross-talks are increasing by a factor

of 2 if compared with the cross-talks in the nominal operation of the chamber in the double-gap mode. Still this cross-talk probability remains quite small, well within the requirements of the LHCb Muon System.

Table7. Cross-talk probabilities in the single-gap and the double-gap modes. Threshold = 30 mV.

Mode	Cross-talk with a neighbour pad, %			
	HV^{D}_{nom}	HV^{D}_{nom}+100 V	HV^{S}_{nom}	HV^{S}_{nom}+100V
Double-gap	2	4	-	-
Single-gap	1	2	4	8

6. Tests of WPC-9 with the SONY++ option for the FE electronics

All the results presented in section 5 were obtained with the PNPI FE electronics. Also, we have performed the beam tests of the WPC-9 prototype operating in the double-gap mode with the SONY++ FE electronics described in section 3. As it was already mentioned in section 5, the input impedance and the signal parameters in SONY++ are quite similar to those in the PNPI FE electronics. Therefore, we could expect similar performance of the chamber equipped with these two options of the FE electronics. Indeed, this expectation was confirmed by the experiment.

Figures 12 to 14 show the HV-dependence of the TDC mean time, the time resolution, and the efficiency measured with the SONY++ and PNPI FE electronics. One can see that all the dependencies are nearly identical for these two options. Figure 15 presents the cross-talk probabilities vs HV. Again, these probabilities proved to be similar for both options. Moreover, the cross-talk between non-neighboring pads proved to be negligible for the SONY++ option while it becomes visible for the PNPI FE electronics option at the highest HV-values. Note, however, that in our case the non-neighboring channels were connected to different chips (see Figure 3a). Therefore, we can not judge so far on the cross-talks inside the chip on the sensitivity level below 1%. On the other hand, the SONY++ data demonstrates that the cross-talks between the non-neighboring pads inside the chamber are close to zero even at the highest HV-values. The appearance of such cross-talks at the highest HV-values

in the case of the PNPI FE electronics is most probably explained by the cross-talks in the main amplifier due to very large signals leading to the overloading of the amplifier.

Concluding this part we may say that the SONY++ option of the FE electronics demonstrated very good performance, identical to performance of the PNPI FE electronics.

Summary

The design of the WPC-8 and WPC-9 prototypes allowed to operate them both in the double-gap and also in the single-gap modes. The performance of these chambers in the double-gap mode was similar to that of the previously described WPC-7 prototype. The efficiency plateau in a 20 ns time window was 480V and 440V for the pad size 4x16 cm^2 and 8x16 cm^2, respectively. Also similar were the cross-talk probabilities. An important observation was high detection efficiency of the chambers operating in the single-gap mode, though with the efficiency plateau reduced by 150V with respect to the double-gap mode. The efficiency of the single-gap chamber operating at the nominal HV-value for the double-gap chamber proved to be around 95%, and it could be restored completely by rising the HV by 150V. From this observation it is concluded that it would be very important to have separate HV-suppliers for each gap. This would allow to operate the double-gap chambers in a single-gap mode, if any problem appears in one of the gaps, thus increasing substantially the redundancy of the Muon System.

The tests of the SONY++ readout option based on the SONY chip with an active adapter at the input demonstrated very good performance of this option, practically identical to that with the PNPI FE electronics based on discrete elements. The SONY++ option is inexpensive and fits well the geometry of the muon chambers in the outer regions, so it can be a possible solution for these regions. There is still some concern on the radiation hardness of the SONY chip as it was not yet tested at high radiation dozes.

Acknowledgments

The authors express their gratitude to the LHCb muon group helping in preparations of the beam tests at CERN. In particular, we are thankful to B. Schmidt, W. Riegler, T.Schneider, A.Kachtchouk who provided the data acquisition and beam trigger systems, the gas supply line, and other equipment needed in the test run. Many thanks to H.J. Hilke for permanent support of this work.

References

1. B.Bochin, S.Guets, V.Lazarev, N.Saugidova, E.Spiridenkov, An.Vorobiev, A.Vorobyov
Beam tests of WPC-7 prototype of the wire pad chambers for the LHCb Muon System.
LHCb 2000-102 Muon 24th October 2000

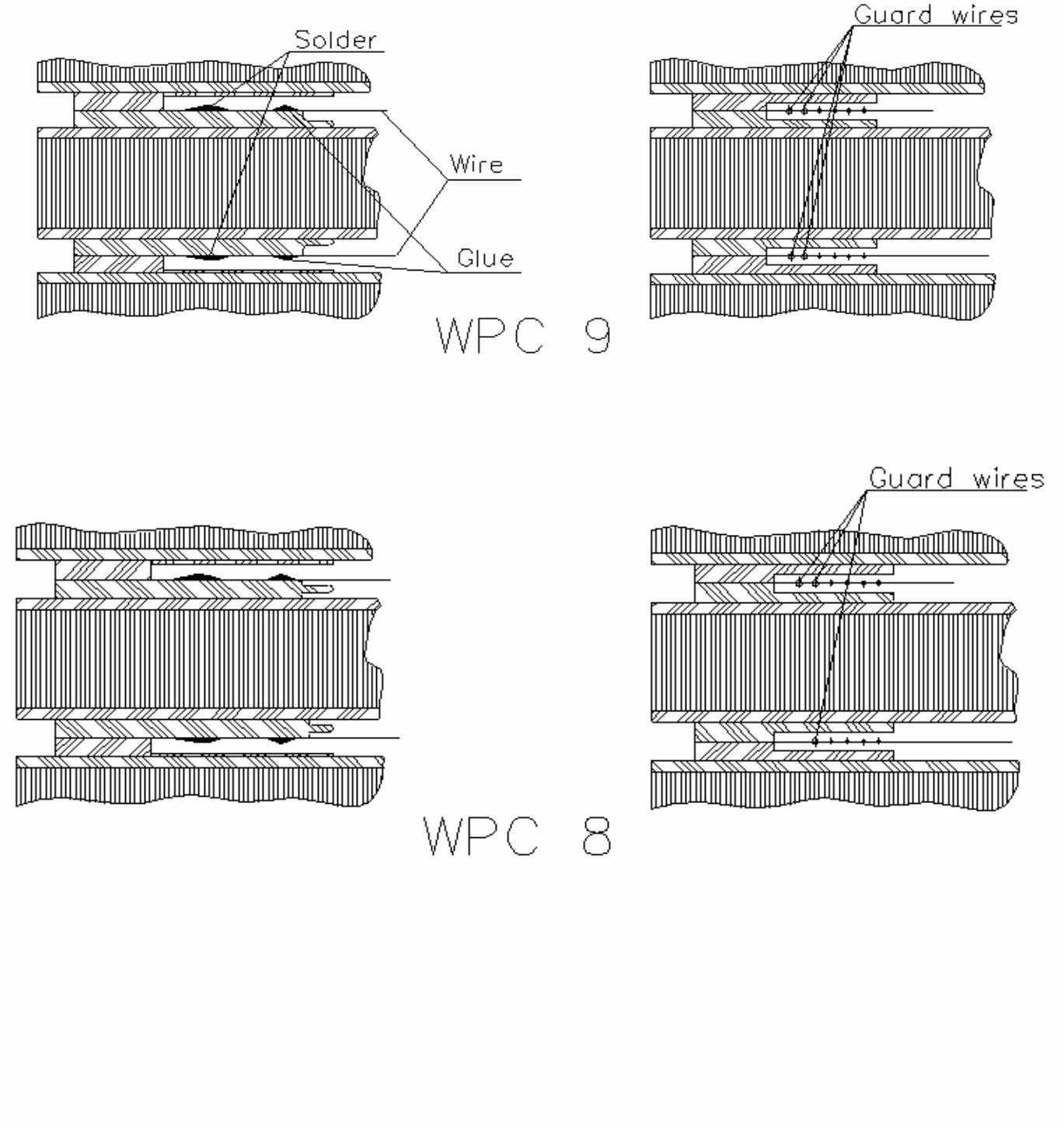

Figure 1. Schematic view of the WPC-8 and WPC-9 prototypes. Left-side figures show the shape of wire fixation bars. Right-side figures illustrate the guard wire (∅90μm) geometry.

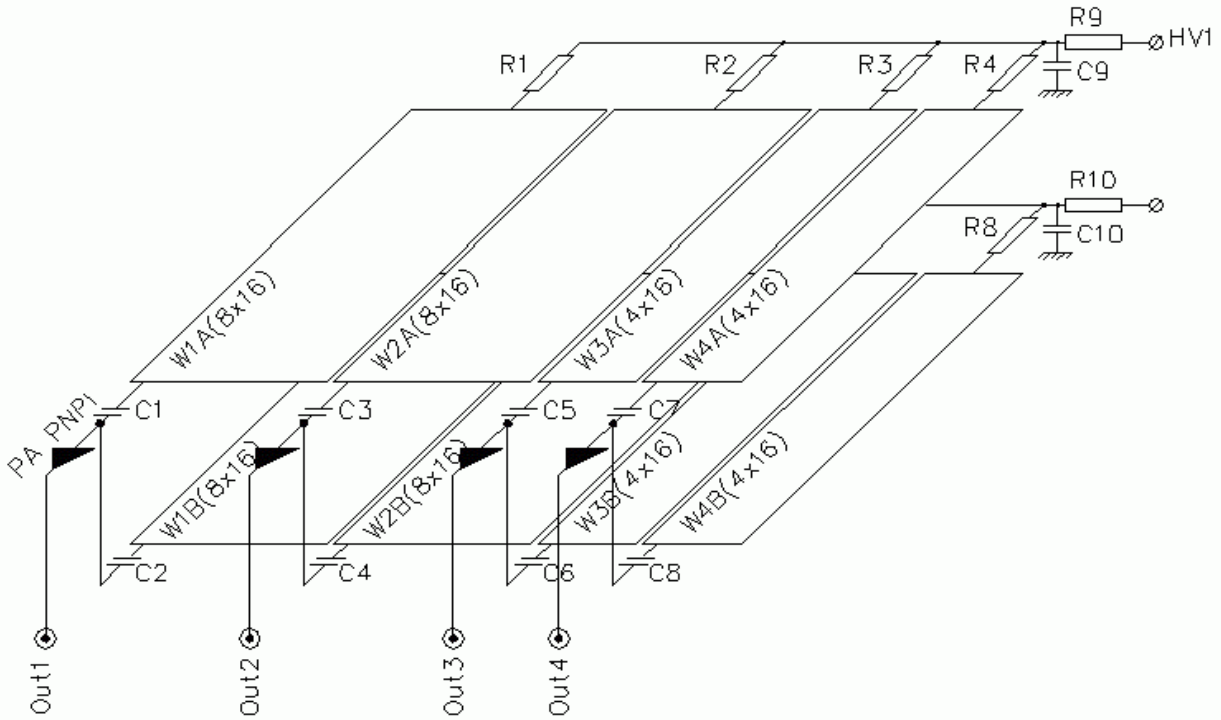

Figure 2a. Double-gap option.

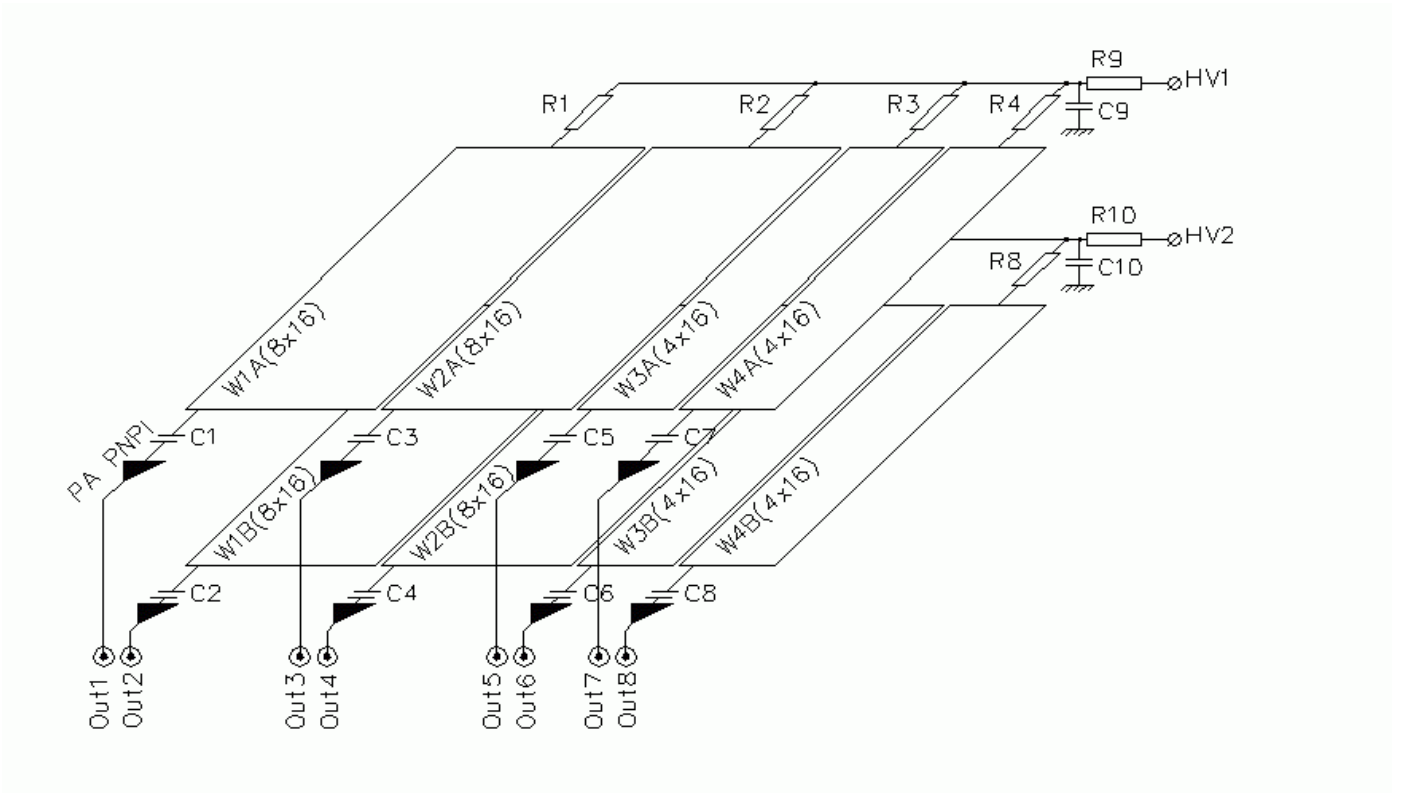

Figure 2b. Single-gap option.
C1÷C10=1nF, R1÷R8=1.5MΩ, R8÷R10=2.2MΩ in both options.

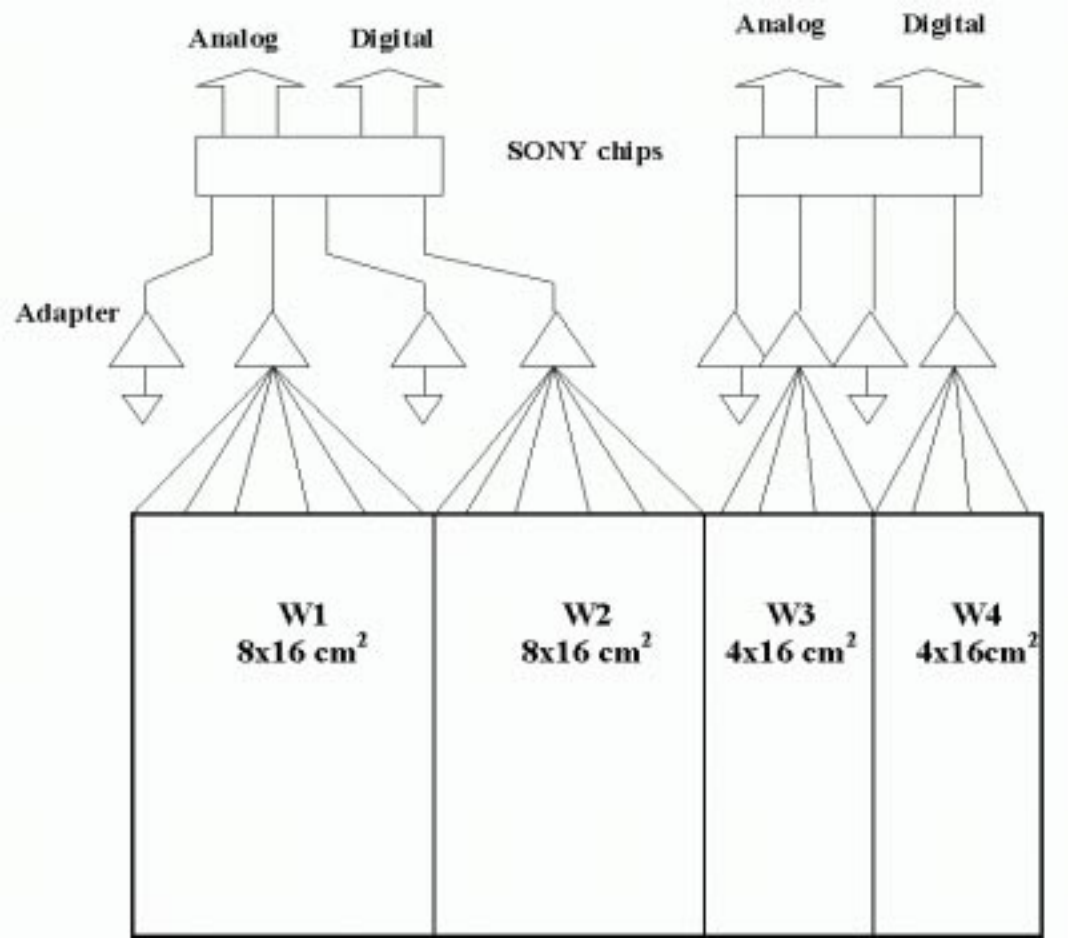

Figure 3a. Scheme of the SONY++ readout option.

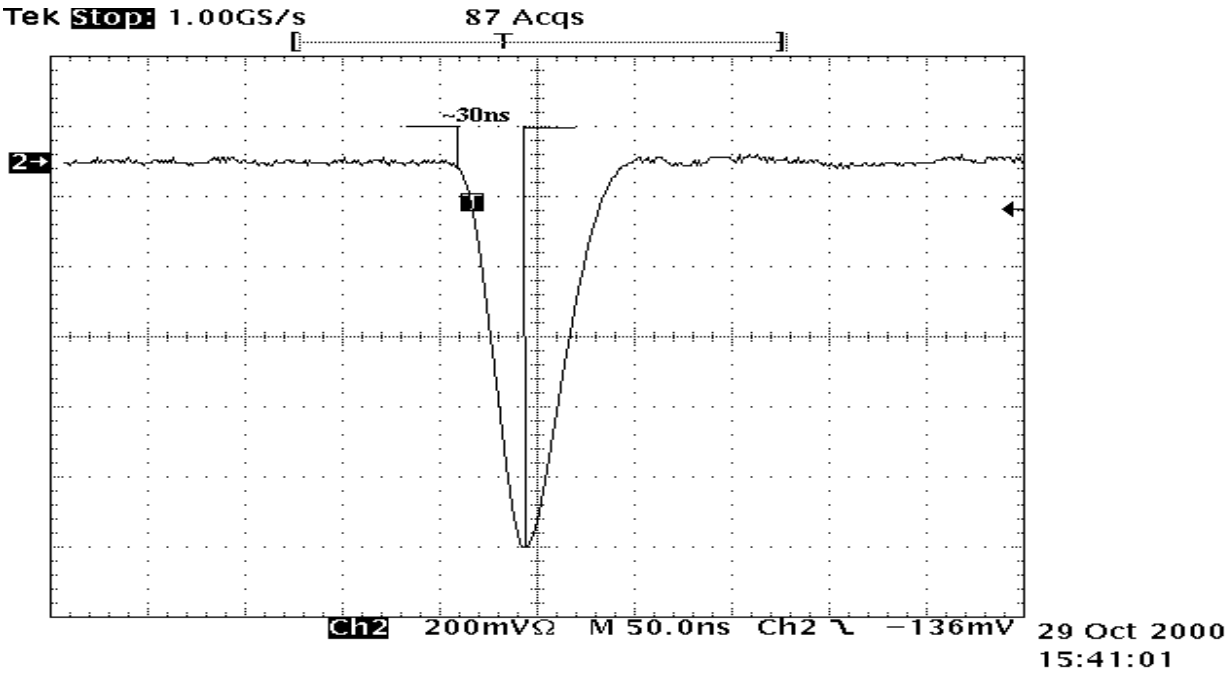

Figure 3b. Signal shape at the analog output of the SONY++ chip.
Pad W1 (8x16 cm^2).

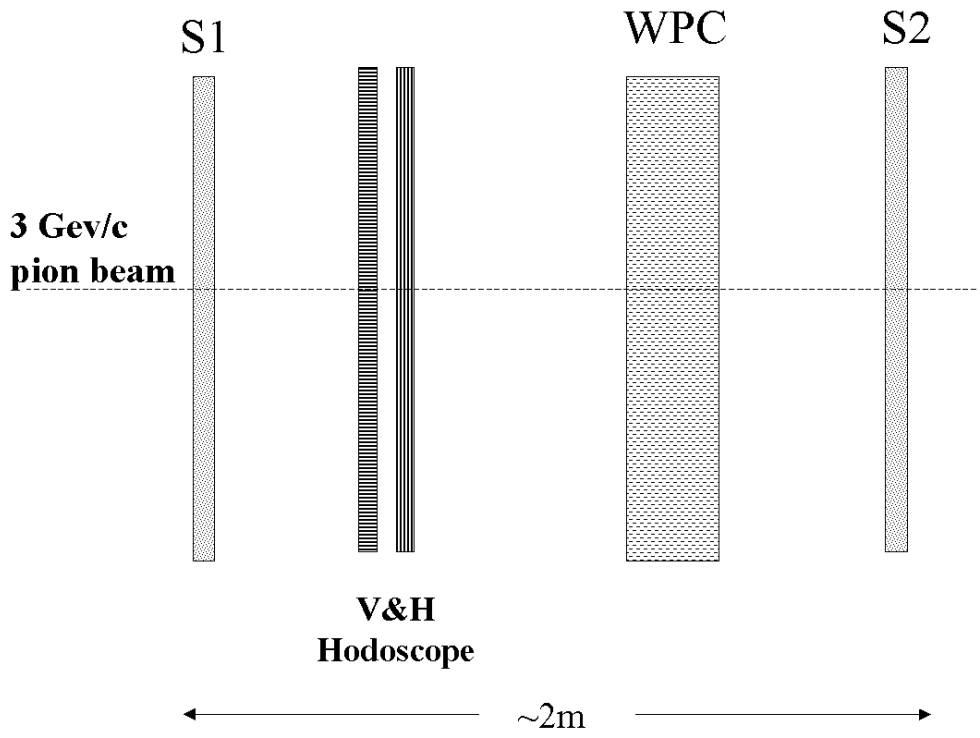

Figure 4. Experimental setup.

S1 – scintillator counter 15x15cm^2
S2 – scintillator counter 20x20cm^2
V&H Hodoscope – 8x8 scintillator counters 1x8cm^2

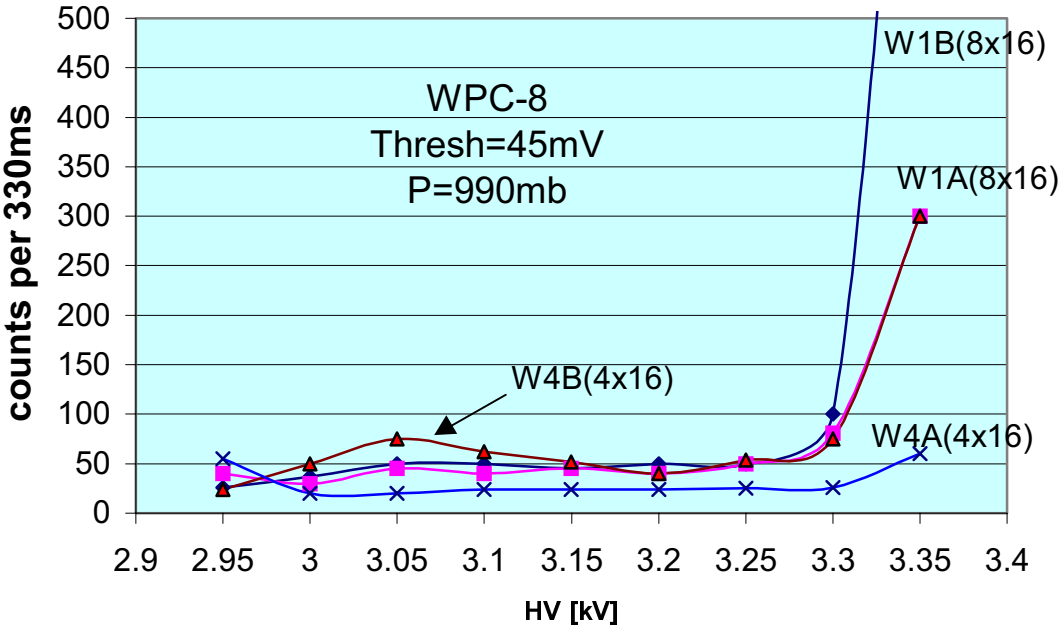

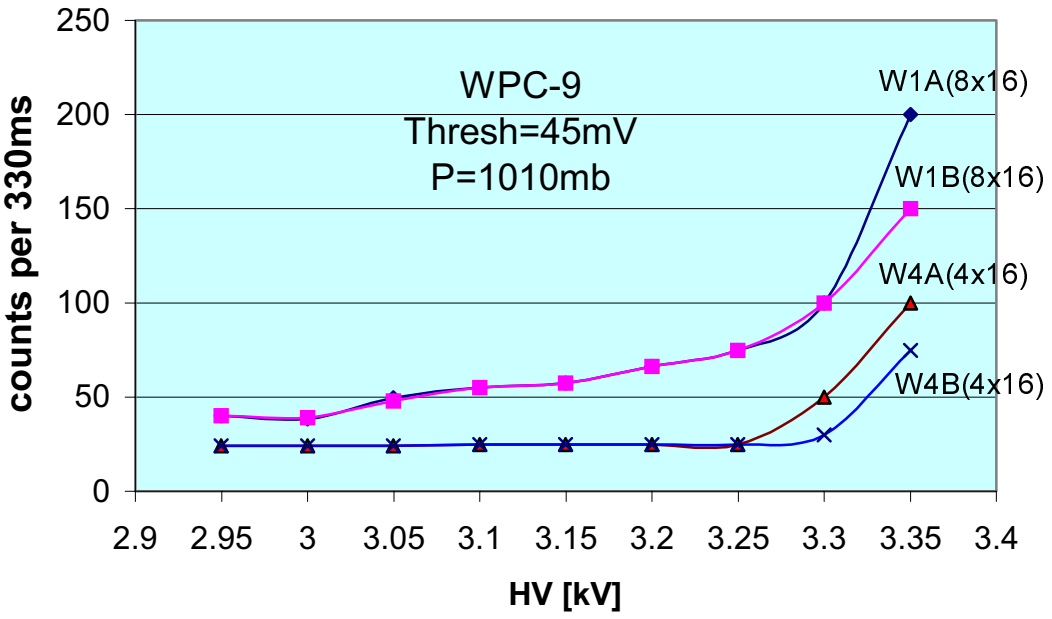

Figure 5. Noise counting rates vs HV measured with WPC-8 and WPC-9 operating in the separate gaps mode.

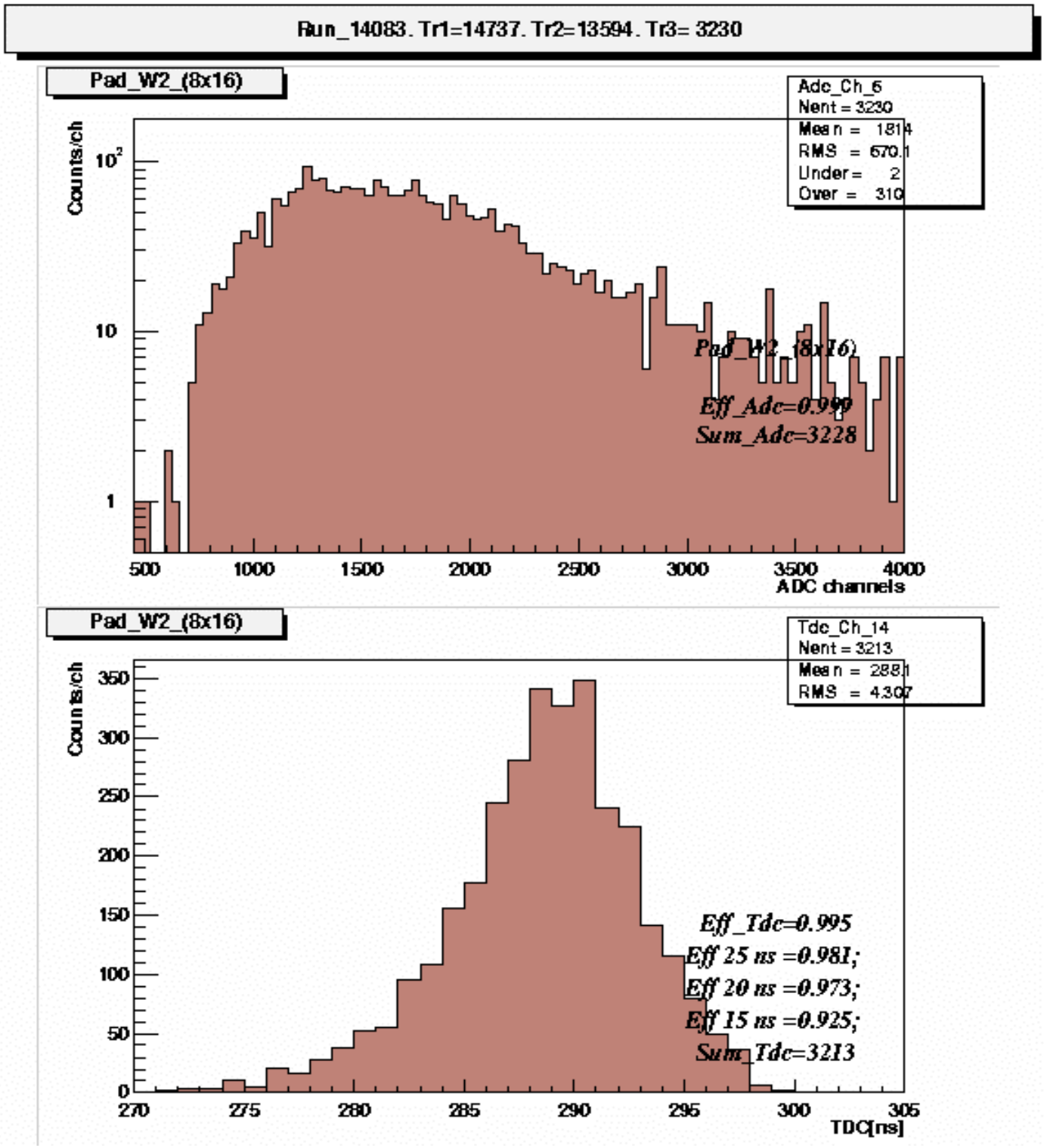

Figure 6. The ADC and TDC spectra of the signals from pad W2(8x16cm^2) in the double-gap WPC-9 measured at HV=3.0 kV. The ADC pedestal is on channel 260. The discriminator level is Th=35mV. The beam spot is selected by hodoscope counters to be inside the pad size.

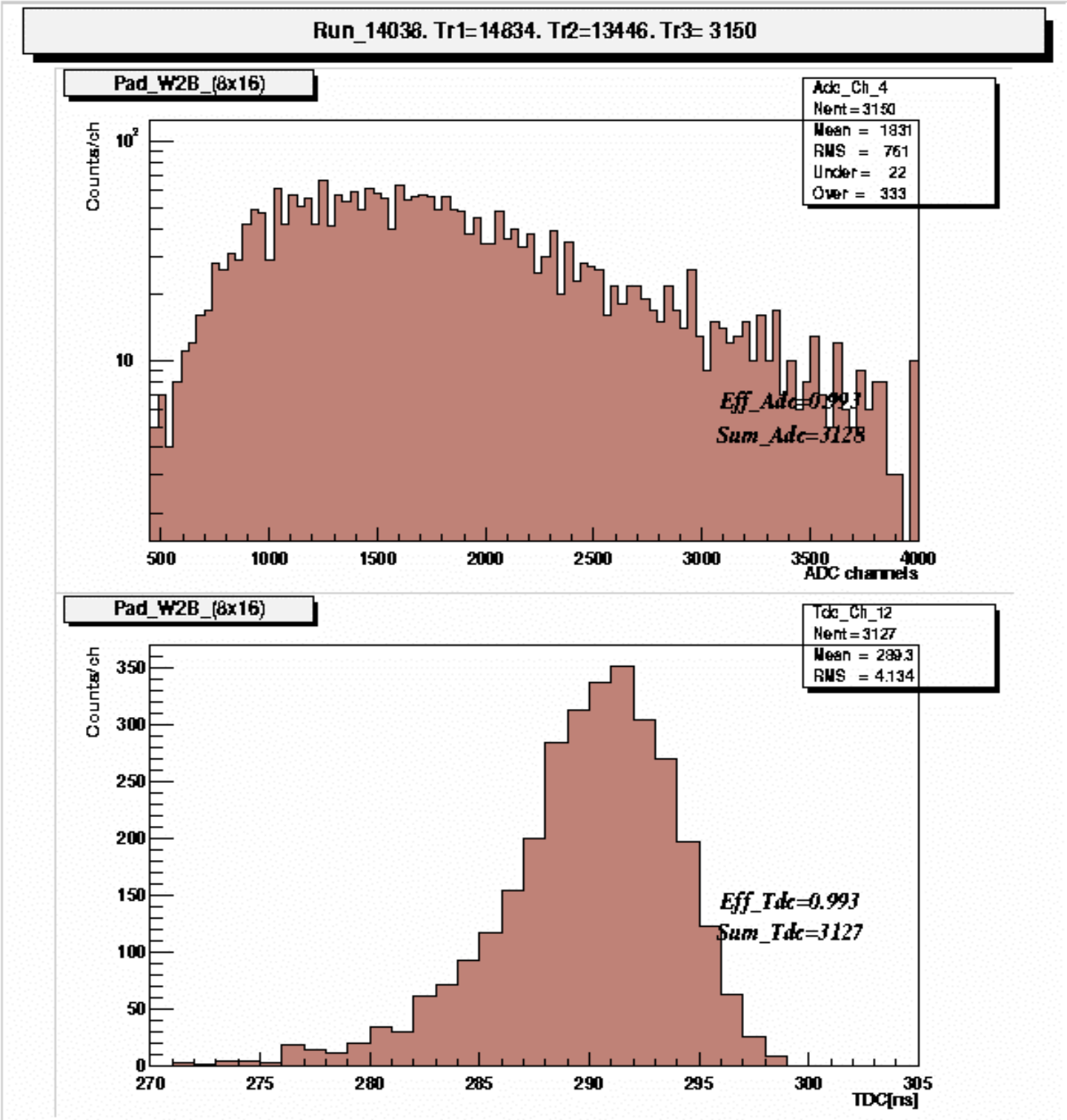

Figure 7. The ADC and TDC spectra of the signals from pad W2 (8x16cm^2) in the single-gap WPC-9 measured at HV=3.15 kV. Th=45mV.

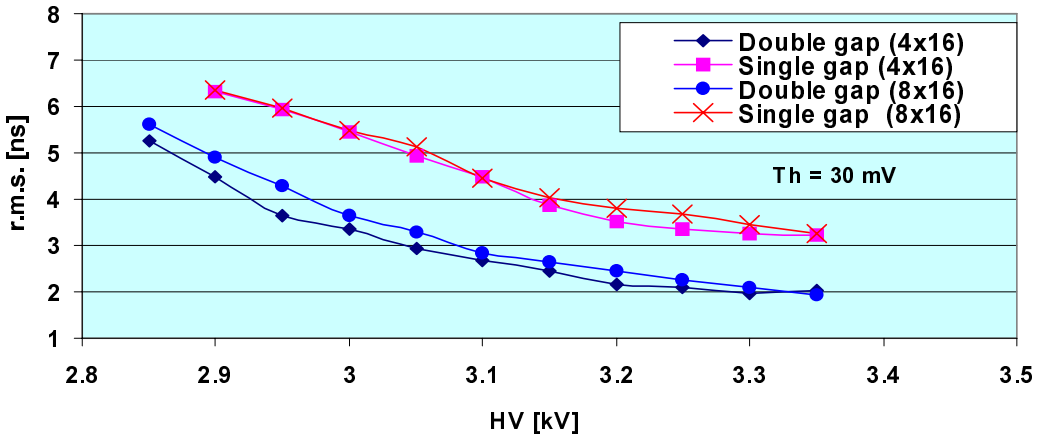

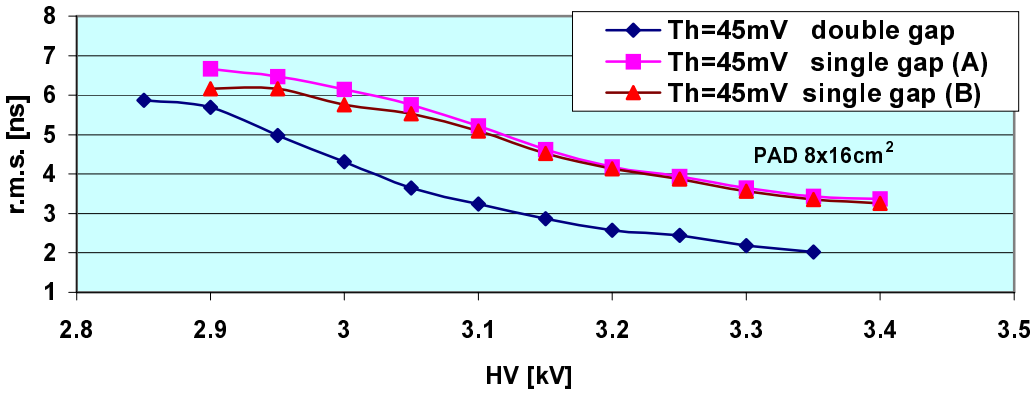

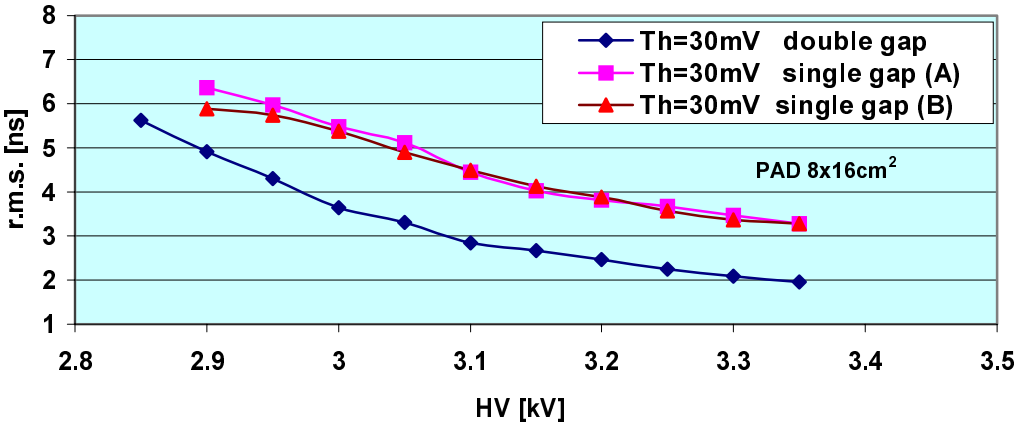

Figure 8. Time resolution vs HV for single-gap and double-gap WPC-9 for various pad sizes and thresholds.

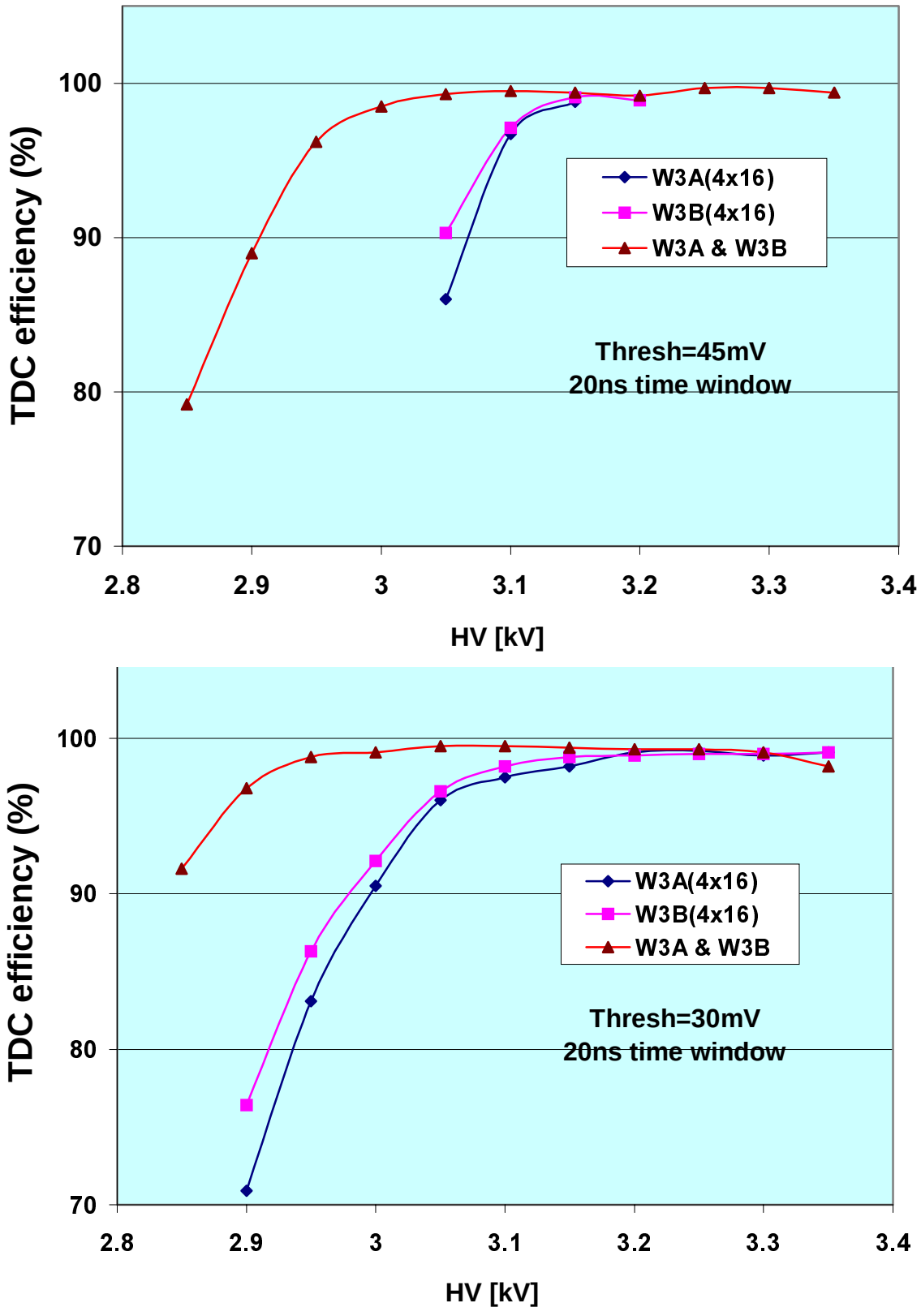

Figure 9. Detection efficiency of WPC-9 operating in the double-gap and single-gap modes. Pad size 4x16 cm^2 .

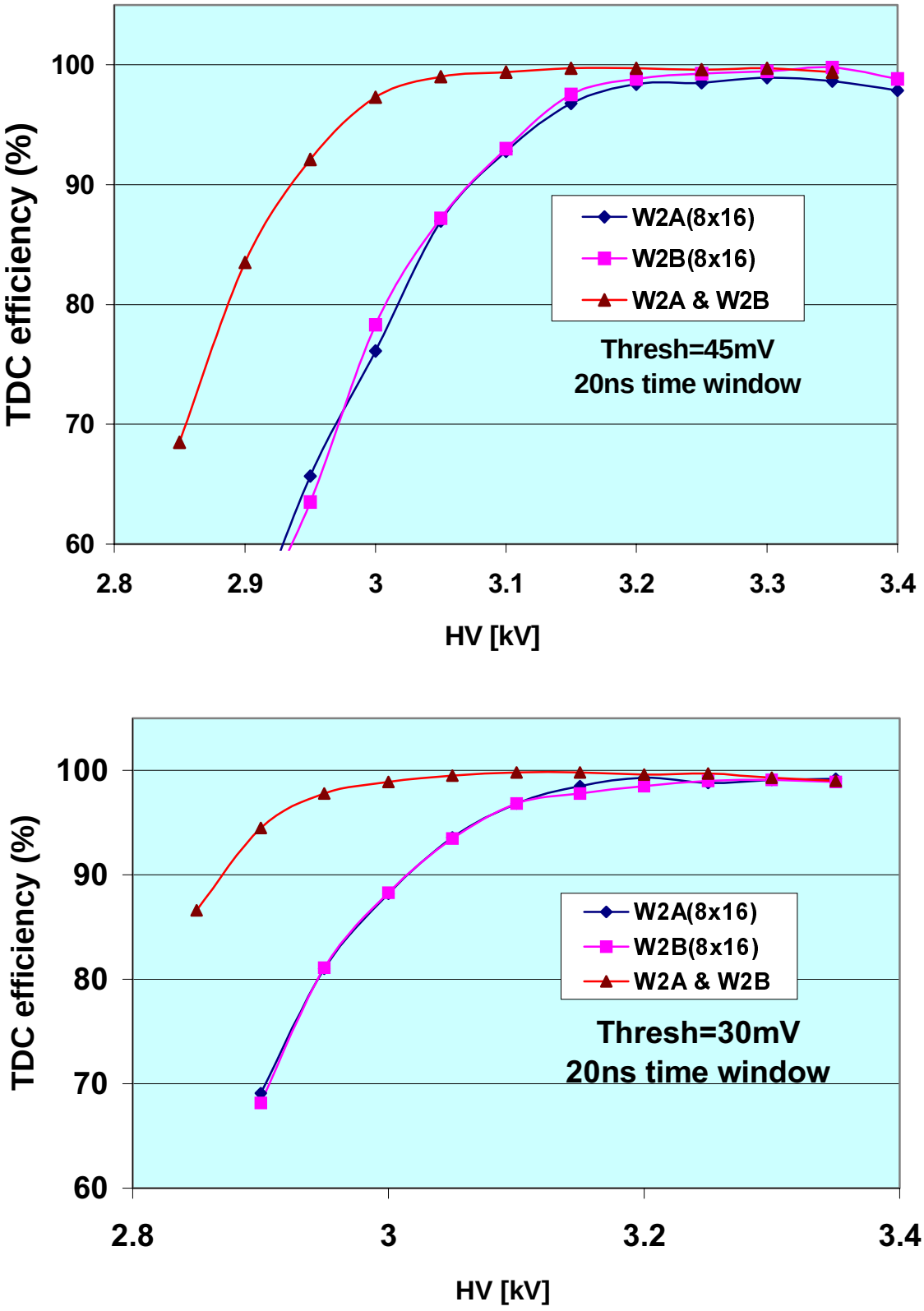

Figure 10. Detection efficiency of WPC-9 operating in the double-gap and single-gap modes. Pad size 8x16 cm^2.

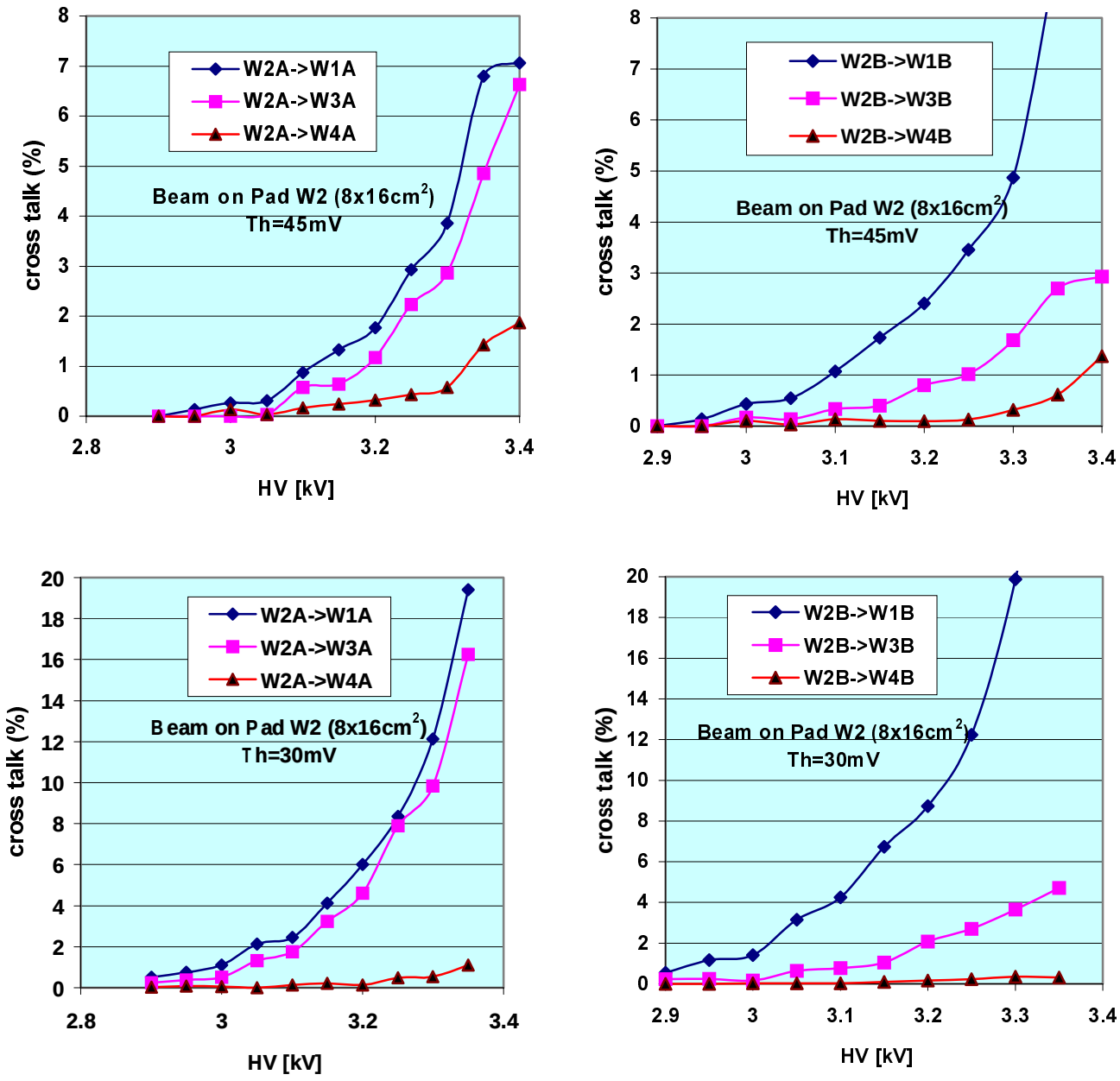

Figure 11. Cross-talk probabilities vs HV in WPC-9 operating in the single-gap mode.

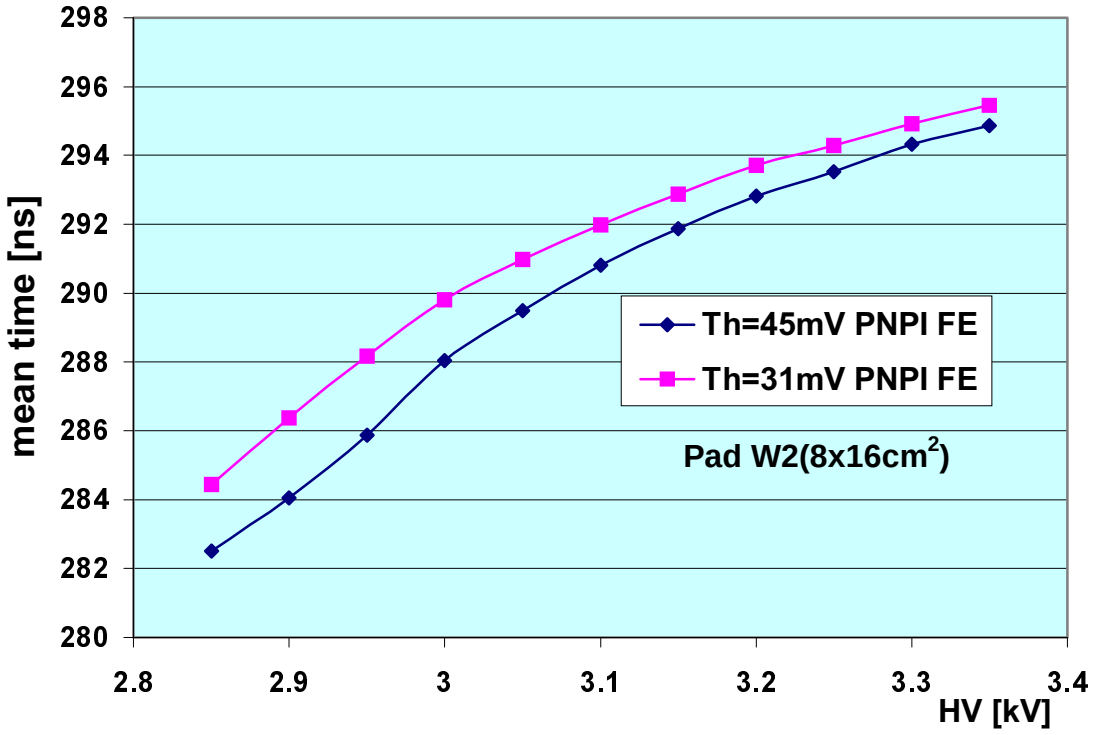

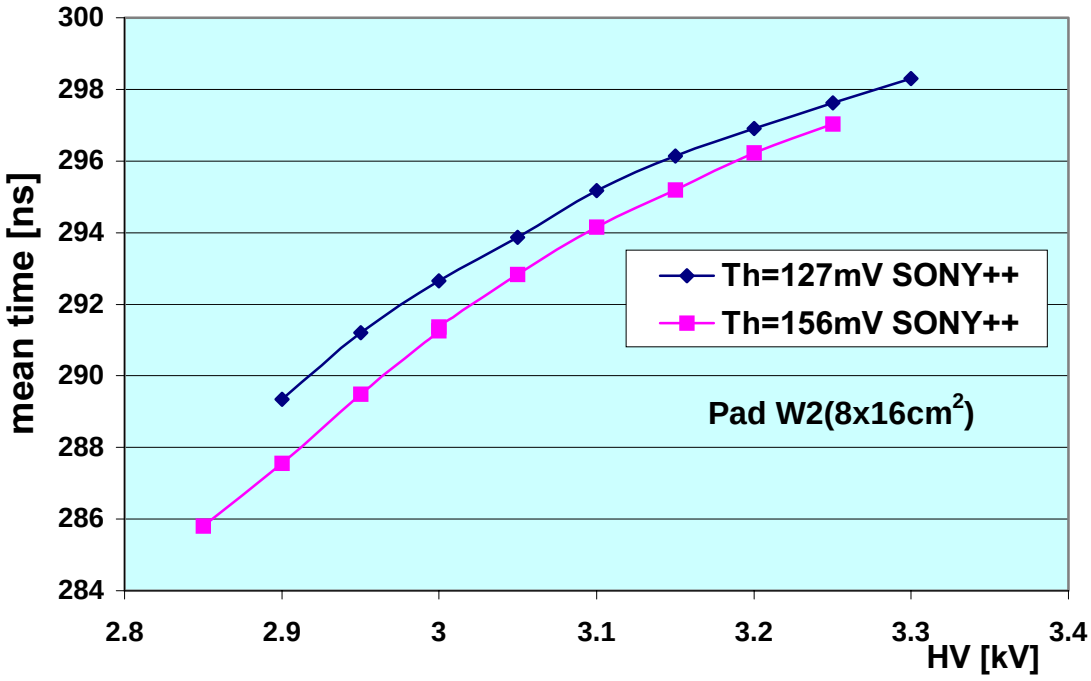

Figure 12. TDC mean time vs HV for PNPI and SONY++ FE electronics. Measurements with WPC-9 operating in the double-gap mode.

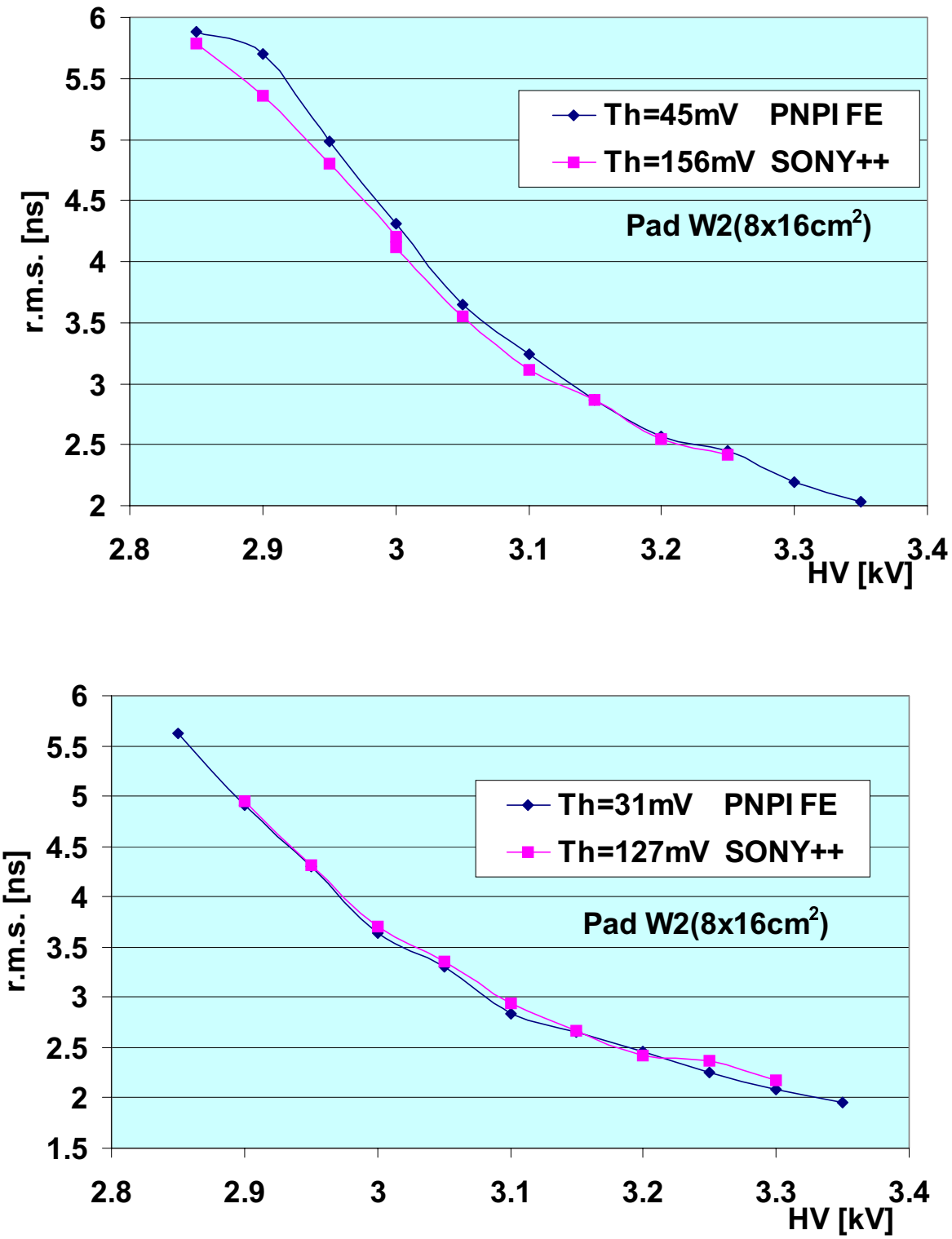

Figure 13. Time resolution vs HV for SONY++ and PNPI FE electronics. WPC-9. Double-gap mode.

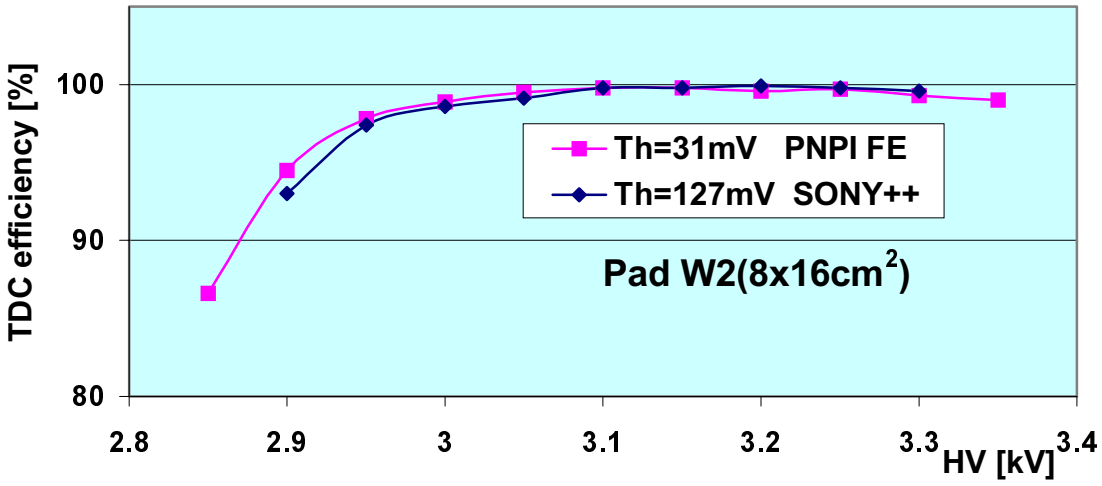

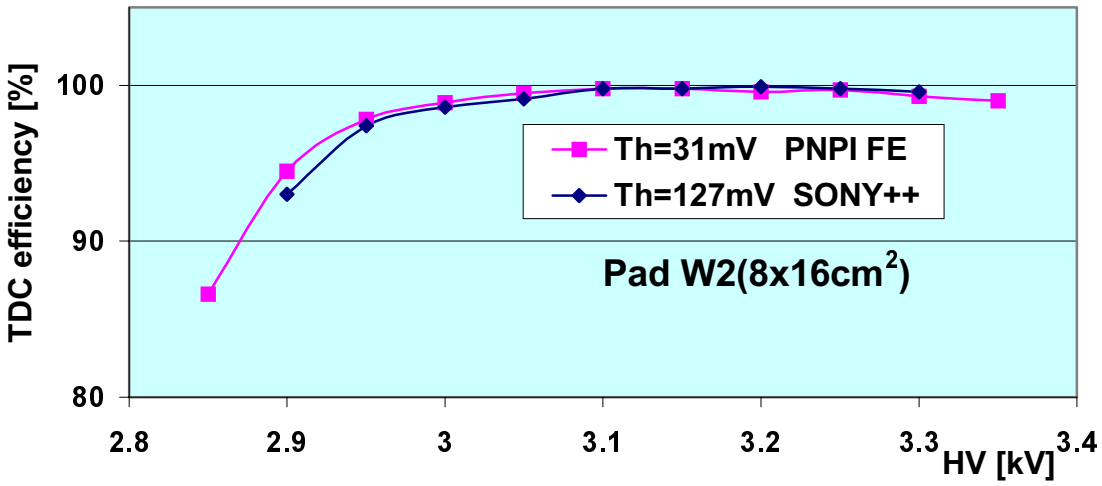

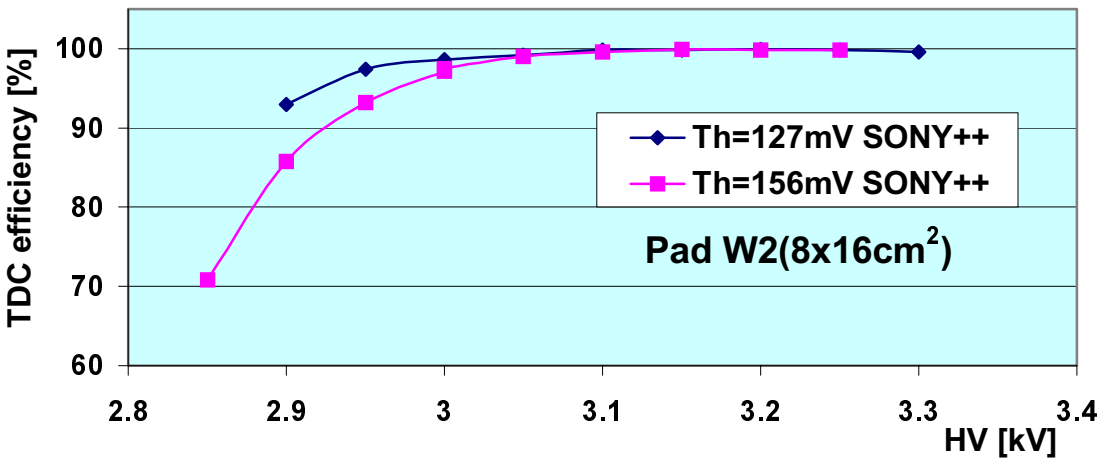

Figure 14. TDC efficiency in 20 ns time window vs HV for SONY++ and PNPI FE electronics. WPC-9. Double-gap mode.

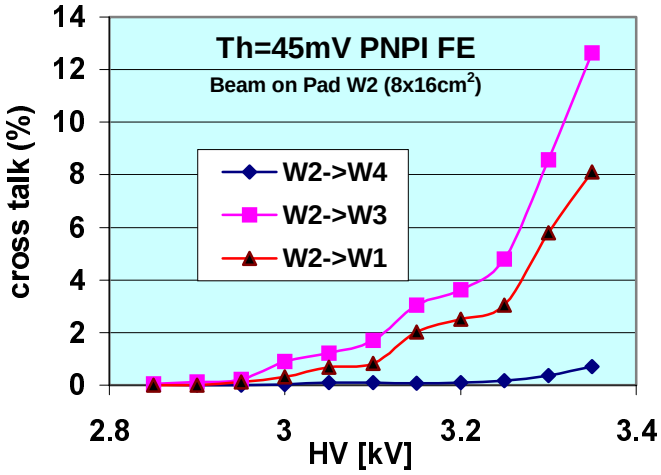

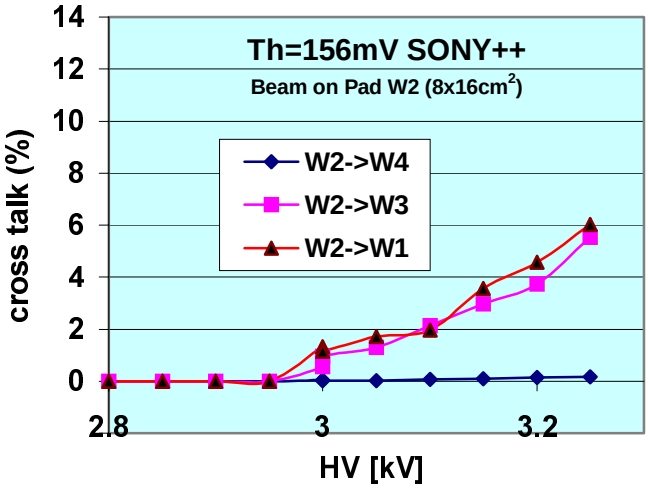

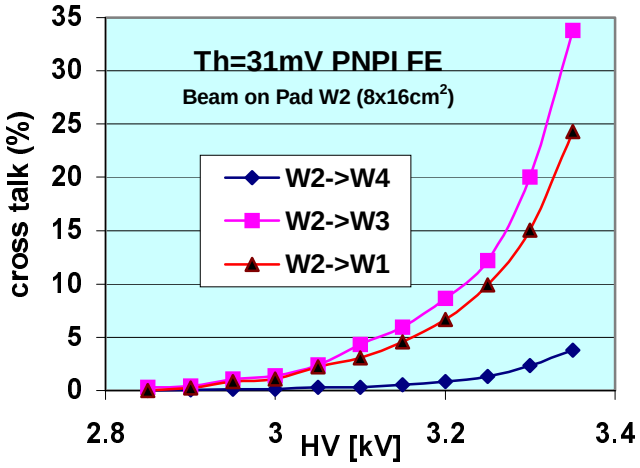

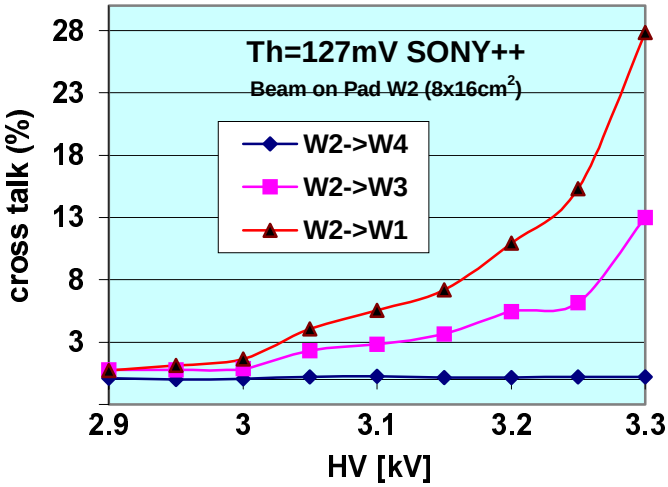

Figure 15. Cross-talk probability for SONY++ and PNPI FE electronics. Beam spot is inside the pad W2(8x16cm^2). WPC-9. Double-gap mode.